Journal of Porphyrins and Phthalocyanines
J. Porphyrins Phthalocyanines 2014; **18**: 1–8
DOI: 10.1142/S1088424614500734

Published at http://www.worldscinet.com/jpp/

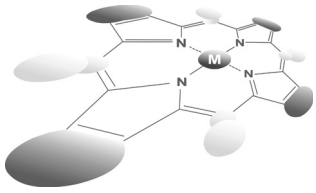

Meso-dichlorophenyl substituted Co(III) corrole: A selective electrocatalyst for the two-electron reduction of dioxygen in acid media, X-ray crystal structure analysis and electrochemistry

Jijun Tang[a], Zhongping Ou*[a◊], Lina Ye[a], Minzhu Yuan[a], Yuanyuan Fang[b◊◊], Zhaoli Xue[a◊] and Karl M. Kadish*[b◊]

[a] *School of Chemistry and Chemical Engineering, Jiangsu University, Zhenjiang 212013, P. R. China*
[b] *Department of Chemistry, University of Houston, Houston, TX 77204-5003, USA*

Dedicated to Professor Nagao Kobayashi on the occasion of his 65th birthday

Received 29 July 2014
Accepted 28 August 2014

ABSTRACT: A cobalt(III) corrole, represented as $(Cl_2Ph)_3CorCo(PPh_3)$, where $(Cl_2Ph)_3Cor$ is the trianion of 5,10,15-tri(2,4-dichlorophenyl)corrole, was synthesized and characterized as to its electrochemical and spectroelectrochemical properties. Single-crystal structure analysis showed the corrole to be monoclinic and have a space group P21/c with $a = 13.441(3)$, $b = 28.058(6)$, $c = 27.584(6)$ Å, $\alpha = 90$, $\beta = 92.75(3)$, $\gamma = 90°$, $M_r = 1144.38$, $V = 1039.1(4)$ Å^3, $Z = 8$, $D_c = 1.463$ mg/cm^3, $\mu = 0.816$, $F(000) = 4644$, $R_{int} = 0.0447$, $R(I > 4\sigma(I)) = 0.0769$, $wR(I > 4\sigma(I)) = 0.2104$, R(all data) = 0.1214 and wR(all data) = 0.2705. The compound was also examined as a catalyst for the electroreduction of dioxygen when coated on an edge-plane pyrolytic graphite electrode in 1.0 M $HClO_4$. Cyclic voltammetry and linear sweep voltammetry with a rotating disk electrode (RDE) or a rotating ring disk electrode (RRDE) were utilized to evaluate the catalytic activity of the corrole and elucidate the products of reduction, H_2O or H_2O_2. Analysis of the data shows exclusively a two-electron transfer process to give 100% H_2O_2 as the product and no H_2O was detectable.

KEYWORDS: cobalt corrole, crystal structure, electrochemistry, catalytic property for dioxygen reduction.

INTRODUCTION

Corroles and metallocorroles have continued to attract a great deal of interest [1–5], in part because these compounds have been shown to have potential applications as catalysts for a variety of reactions [6–14]. One of the most frequently studied groups of metallocorroles are the cobalt(III) derivatives which have been characterized as to their spectral and electrochemical properties under many different solution conditions [1, 2].

Part of our own recent research efforts in this area have focused on the synthesis, characterization and catalytic properties of substituted cobalt corroles [9–22]. In the present paper, the synthesis, structural characterization, electrochemistry and spectroelectrochemistry of a newly synthesized *meso*-dichlorophenyl substituted cobalt corrole are described. The examined compound is represented as $(Cl_2Ph)_3CorCo(PPh_3)$, where $(Cl_2Ph)_3Cor$ is the trianion of 5,10,15-tri(2,4-dichlorophenyl)corrole. Electrochemical and spectroelectrochemical properties of the compound were examined in dichloromethane, benzonitrile and pyridine containing 0.1 M TBAP as supporting electrolyte.

When adsorbed on a graphite electrode, cobalt corroles are able to catalyze the electroreduction of oxygen *via* a

[◊]SPP full and [◊◊] student member in good standing

*Correspondence to: Zhongping Ou, email: zpou2003@yahoo.com, tel/fax: +86 511-8879-1800; Karl M. Kadish, email: kkadish@uh.edu, tel: +1 (713)-743-2740, fax: +1 (713)-743-2745

2e or 4e transfer process to produce H_2O_2 or H_2O as a final product [9–11, 15, 22–24]. We previously demonstrated that the type and location of substituents on the three phenyl rings of a triphenylcorrole will significantly affect the catalytic activity of the compound towards the reduction of O_2 [11, 12, 22]. We also suggested that bulky substituents at the *ortho*-positions of the three *meso*-phenyl rings of a cobalt corrole would prevent π–π interactions of the macrocycles on the electrode surface and thus block dimerization (needed for a 4e reduction of O_2) due to steric hindrance [11, 22]. This is confirmed in the present paper which reports the electrochemical properties and catalytic activity of $(Cl_2Ph)_3CorCo(PPh_3)$ as a catalyst for O_2 reduction.

RESULTS AND DISCUSSION

X-ray structure of $(Cl_2Ph)_3CorCo(PPh_3)$

The complex crystalizes in a monoclinic P21/c space group, with two crystallographically independent cobalt complex molecules and solvent. An ORTEP plot is depicted in Fig. 1 where one of the two conformations of the compound is shown. The structural refinement data are given in Table 1 and selected bond lengths and angles are listed in Table 2.

Although significant disorder is found for most of the dichlorophenyl groups and dichloromethane molecules in the structure, the colbalt-corrole-triphenylphosphine core is well-defined. The Co–N bond lengths of the two molecules vary from 1.862(5) to 1.884(5) Å and the Co–P distances are 2.2167(17) and 2.2158(17) Å, respectively. It is interesting to note that the dichlorophenyl groups opposite to the unsubstituted positions of $C_6H_3Cl_2$ are not disordered and the chlorine, Cl3 (in Fig. 1) or (Cl9 in the second molecule) is oriented *cis* to the phosphorus of the bound PPh_3. The triphenylphosphine ligand is tilted towards the unsubstituted phenyl positions as evidenced by a smaller angle of 93.5° for N1–Co1–P1 and N4–Co1–P1 as compared to 103.5° for N2–Co1–P1 and N3–Co1–P1. The central cobalt ion is displaced from the corrole mean plane by 0.23 Å.

Table 1. Crystal data and structure refinement for $(Cl_2Ph)_3CorCo(PPh_3)$

Empirical formula	$C_{56.25}H_{35}Cl_8CoN_4O_{0.25}$ P
Formula weight	1144.38
Temperature	173(2) K
Wavelength	0.71073 Å
Crystal system	monoclinic
Space group	P 21/c
Unit cell dimensions	a = 13.441(3) Å α = 90° b = 28.058(6) Å β = 92.75(3)° c = 27.584(6) Å γ = 90°
Volume	1039.1(4) Å^3
Z	8
Density (calculated)	1.463 mg/cm^3
Absorption coefficient	0.816 mm^{-1}
F(000)	4644
Crystal size	0.250 × 0.250 × 0.130 mm^3
Theta range for data collection	3.365 to 26.027°
Index ranges	-16 ≤ h ≤ 14, -29 ≤ k ≤ 33, -34 ≤ l ≤ 20
Reflections collected	49226
Independent reflections	20215 [R(int) = 0.0447]
Completeness to theta = 25.242°	99.0%
Refinement method	full-matrix least-squares on F^2
Data/restraints/parameters	20215/0/1111
Goodness-of-fit on F^2	1.113
Final R indices [$I > 4\sigma$ (I)]	R_1 = 0.0769, wR_2 = 0.2104
R indices (all data)	R_1 = 0.1214, wR_2 = 0.2705
Extinction coefficient	0.0018(2)
Largest diff. peak and hole	1.358 and -1.611 eÅ^{-3}

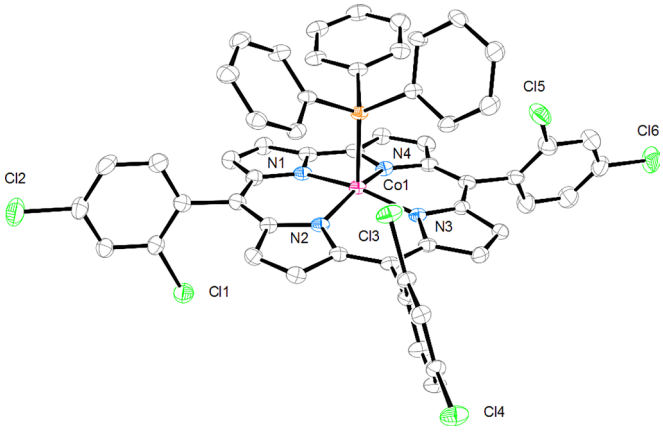

Fig. 1. An ORTEP plot of the complex with thermal ellipsoids at 25% probability level. Hydrogen atoms were omitted for clarity. The Cl1/Cl2 and Cl5/Cl6 are disordered over at least two positions. The Cl1 and Cl5 are positioned up or down the corrole mean plane. The plot represents one of the potential conformations

UV-visible spectra

Electronic absorption spectra of $(Cl_2Ph)_3CorCo(PPh_3)$ in CH_2Cl_2, PhCN and pyridine are illustrated in Fig. 2 and a summary of spectral data in the three solvents is given in Table 3. In CH_2Cl_2 and PhCN, neutral $(Cl_2Ph)_3CorCo(PPh_3)$ exhibits a split Soret band located between 381 and 411 nm and two weak Q-bands between 554 and 584 nm. However, a

Table 2. Selected bond lengths and angles for $(Cl_2Ph)_3CorCo(PPh_3)$

Molecule 1				Molecule 2			
Bond length, Å		Bond angle, °		Bond length, Å		Bond angle, °	
Co1-N1	1.871 (5)	N1-Co1-N2	89.3 (2)	Co2-N5	1.864 (5)	N5-Co2-N6	90.0 (2)
Co1-N2	1.884 (5)	N1-Co1-N4	81.3 (2)	Co2-N6	1.882 (5)	N5-Co2-N8	80.7 (2)
Co1-N3	1.875 (5)	N2-Co1-N3	94.7 (2)	Co2-N7	1.878 (5)	N6-Co2-N7	94.5 (2)
Co1-N4	1.862 (5)	N3-Co1-N4	89.2 (2)	Co2-N8	1.866 (5)	N7-Co2-N8	89.4 (2)
Co1-P1	2.2167 (17)	N1-Co1-P1	93.54 (15)	Co2-P2	2.2158 (17)	N5-Co2-P2	92.08 (15)
C1-C19	1.404 (9)	N2-Co1-P1	103.38 (15)	C56-C74	1.412 (10)	N6-Co2-P2	103.16 (15)
N1-C1	1.368 (7)	N3-Co1-P1	103.65 (15)	N5-C56	1.366 (8)	N7-Co2-P2	103.76 (15)
N4-C19	1.383 (7)	N4-Co1-P1	93.53 (15)	N8-C74	1.374 (8)	N8-Co2-P2	95.25 (16)

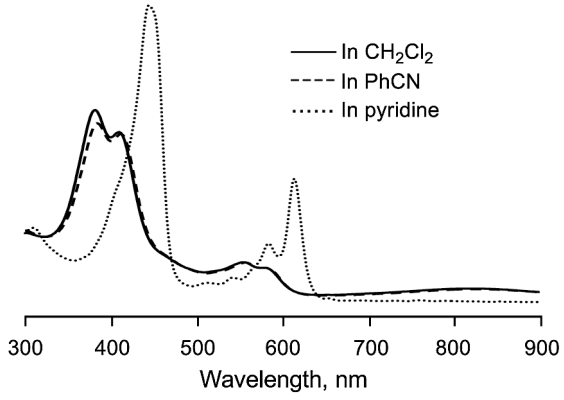

Fig. 2. UV-visible spectra of the neutral cobalt corrole in CH_2Cl_2 (——), PhCN (------) and pyridine (·····) containing 0.1 M TBAP

Table 3. UV-visible spectral data, λ_{max}, nm ($\varepsilon \times 10^{-4}$ $M^{-1}.cm^{-1}$) of $(Cl_2Ph)_3CorCo(PPh_3)$

Solvent	Soret region		Visible region	
CH_2Cl_2	381 (4.05)	409 (3.57)	554 (0.75)	584 (0.60)
PhCN	383 (3.84)	411 (3.60)	557 (0.75)	580 (0.64)
Pyridine		444 (6.35)	584 (1.16)	614 (2.57)

different UV-vis spectrum is exhibited in pyridine where there is a single sharp Soret band at 444 nm and two well-defined Q-bands at 584 and 614 nm (see Fig. 2). This spectrum is consistent with formation of a six-coordinate cobalt(III) corrole, $(Cl_2Ph)_3CorCo(py)_2$, where the original axially bound PPh_3 group has been displaced by a pyridine molecule. Similar UV-vis spectra were previously reported for other six-coordinate cobalt(III) corroles with two pyridine axial ligands [22].

Electrochemistry

Cyclic voltammograms illustrating the oxidations and reductions of $(Cl_2Ph)_3CorCo(PPh_3)$ in CH_2Cl_2, PhCN and pyridine containing 0.1 M TBAP are shown in Fig. 3.

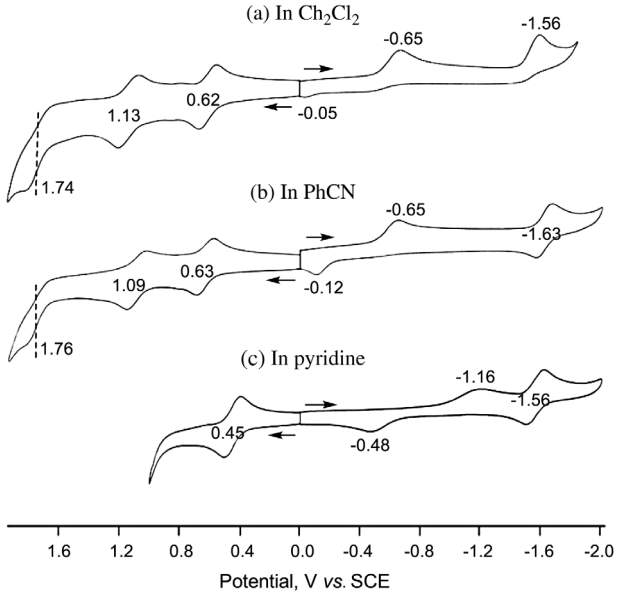

Fig. 3. Cyclic voltammograms of $(Cl_2Ph)_3CorCo(PPh_3)$ in (a) CH_2Cl_2, (b) PhCN and (c) pyridine containing 0.1 M TBAP. Scan rate at 0.10 V/s

The first one-electron reduction is irreversible in all three solvents and located at E_{pc} = -0.65 V in CH_2Cl_2 or PhCN and -1.16 V in pyridine. The irreversibility is due to dissociation of the axially coordinated ligand(s) after electron transfer to generate a four-coordinate Co(II) corrole which is then reoxidized to a four-coordinate Co(III) complex at E_{pa} = -0.05 V in CH_2Cl_2, -0.12 V in PhCN and -0.48 V in pyridine as shown in Fig. 3. The four-coordinate Co(II) corrole can also be reduced to its Co(I) form at more negative potentials [14, 18, 25] and this reaction occurs at $E_{1/2}$ = -1.63 in PhCN, -1.56 V in pyridine and E_{pc} = -1.56 V in CH_2Cl_2.

The second reduction of $(Cl_2Ph)_3CorCo(PPh_3)$ is reversible in PhCN and pyridine but irreversible in CH_2Cl_2 because the electrogenerated Co(I) form of the corrole rapidly reacts with the solvent to give a transient Co(III) σ-bonded CH_2Cl species, as has also been shown

Table 4. Half-wave potentials (V *vs.* SCE) in different solvents containing 0.1 M TBAP

Solvent	Oxidation			Reduction	
	3rd	2nd	1st	1st	2nd
CH_2Cl_2	1.74	1.13	0.62	-0.65[a]	-1.56[a]
PhCN	1.76	1.09	0.63	-0.65[a]	-1.63
Pyridine			0.45	-1.16[a]	-1.56

[a]Peak potential for irreversible reductions at a scan rate of 0.10 V/s.

to occur for other electrogenerated Co(I) corroles [14] and structurally related Co(I) porphyrins [26] where the electrochemistry was carried out in dichloromethane.

The first oxidation of $(Cl_2Ph)_3CorCo(PPh_3)$ is reversible in all three nonaqueous solvents, with $E_{1/2}$ values ranging from 0.45 V in pyridine to 0.63 V in PhCN (see Table 4). This one-electron abstraction is followed by two additional electron abstractions in CH_2Cl_2 and PhCN (Fig. 3), but only one oxidation is observed in pyriding due to the limited positive potential range of this solvent.

It should be noted that dimerization does not occur for $(Cl_2Ph)_3CorCo(PPh_3)$ in CH_2Cl_2 as has been reported for other β-substituted corroles in this solvent [13, 19], and this is attributed to the presence of the bulky Cl_2Ph substituents on the *meso*-positions of the macrocycle, which prevents dimerization.

The electroreduced and electrooxidized corroles were characterized by thin-layer spectroelectrochemistry in PhCN. Examples of the spectral changes are shown in Fig. 4 during the first and second controlled potential oxidations and reductions.

As mentioned above, the neutral Co(III) corrole is characterized by a split Soret band at 383 and 411 nm along with two weak Q-bands at 557 and 583 nm in PhCN. The singly oxidized corrole, which has an unsplit Soret band at 383 nm and a new Q-band at 658 nm (Fig. 4a), can be assigned as a Co(IV) corrole or a Co(III) π-cation radical [22]. However, DFT calculations at the PCM-B3LYP/LanL2DZ/6-31G(d) level show that no metal orbital is involved in the HOMO (Fig. 5a), thus suggesting that the first oxidation of $(Cl_2Ph)_3CorCo(PPh_3)$ is a macrocycle-centered electron-transfer. Further oxidation at an applied potential at 1.30 V then gives the Co(IV) π-cation radical and the spectral changes associated with this reaction are shown in Fig. 4a.

The first controlled potential reduction at -1.00 V generates a Co(II) corrole which has a well-defined Soret band at 428 nm (Fig. 4b). These spectral changes are reversible and reoxidation at a controlled potential of 0.0 V leads to recovery of the initial Co(III) spectrum in PhCN. Similar types of spectral changes have been reported for the Co(III)/Co(II) reaction of other corroles [12, 14, 18, 25] and porphyrins [27, 28] with related structures. The LUMO orbital calculated by DFT (Fig. 5b) is also consistent with a metal-centered reduction upon addition of one electron to the compound.

The second controlled potential reduction of $(Cl_2Ph)_3CorCo(PPh_3)$ at -1.90 V is accompanied by only small spectral changes and has been interpreted in terms of a Co^{II}/Co^{I} electron transfer rather than a corrole ring-centered process, which would be characterized by a decreased intensity Soret band and a broad visible band in the near-IR region of the spectrum.

Electrocatalytic reduction of O_2

Figure 6a illustrates cyclic voltammograms of $(Cl_2Ph)_3CorCo(PPh_3)$ adsorbed on an EPPG disk electrode in 1.0 M $HClO_4$ under N_2 (dashed line) and under air (solid line). Under N_2, there is a small anodic broad

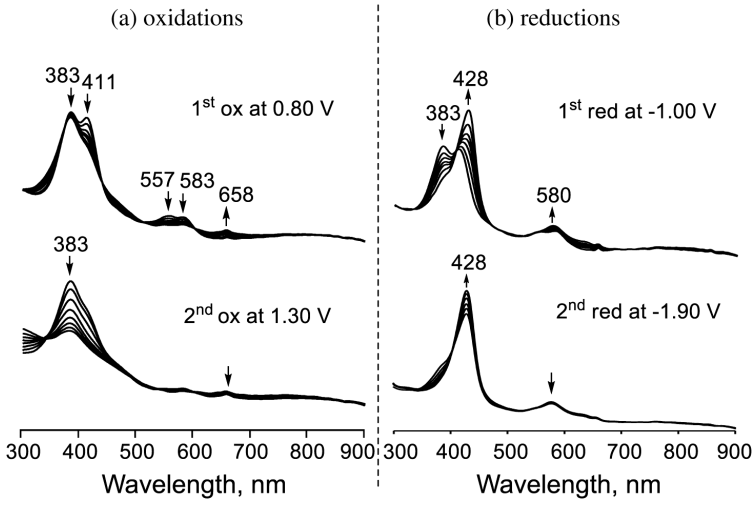

Fig. 4. Thin-layer UV-visible spectral changes of $(Cl_2Ph)_3CorCo(PPh_3)$ during controlled potential reductions and oxidations in PhCN containing 0.1 M TBAP

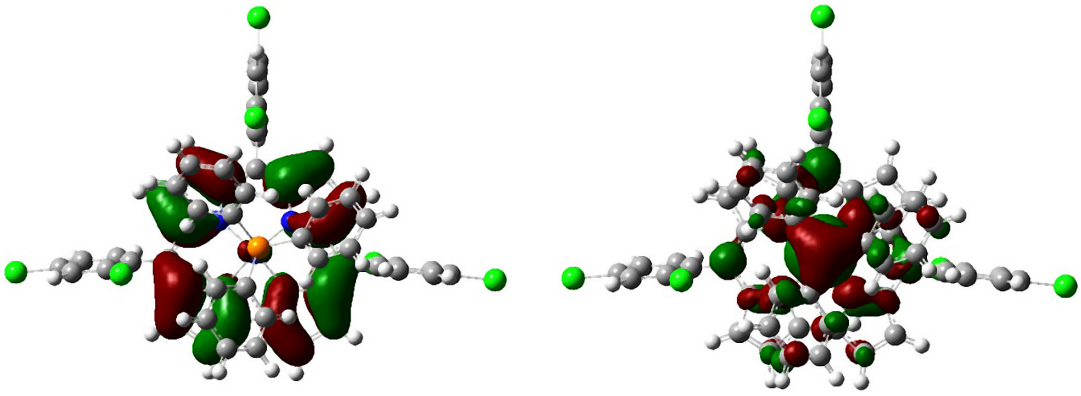

(a) (b)

Fig. 5. (a) HOMO and (b) LUMO orbitals of $(Cl_2Ph)_3CorCo(PPh_3)$ calculated at the B3LYP/6-31G(d) level

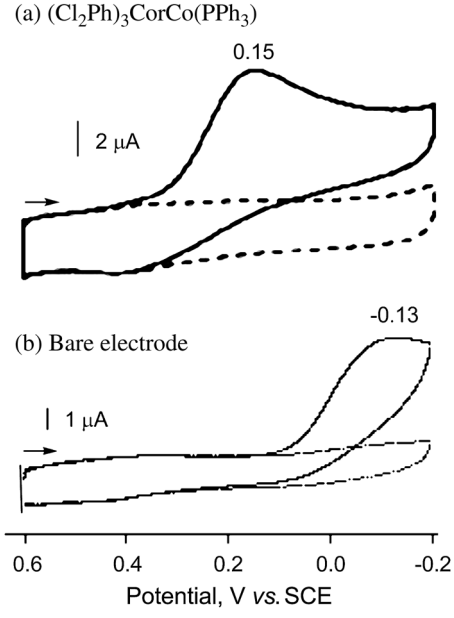

Fig. 6. Cyclic voltammograms of (a) $(Cl_2Ph)_3CorCo(PPh_3)$ absorbed on an EPPG electrode and (b) uncoated bare electrode in 1.0 M $HClO_4$ under N_2 (----) or air (—). Scan rate = 50 mV/s

peak centered at about 0.1 V and no other peaks can be assigned to the corrole between 0.60 and -0.20 V. A different situation occurs in 1.0 M $HClO_4$ under air (solid line in Fig. 6a). Under these conditions, there is an irreversible but well-defined cathodic reduction peak at E_{pc} = 0.15 V for a scan rate of 50 mV/s. As will be shown, this irreversible peak corresponds to the catalytic reduction of dissolved O_2 to give H_2O_2. The dioxygen in solution is also reduced at a bare EPPG electrode without the corrole and this reaction occurs at a more-negative potential of E_{pc} = -0.13 V for a scan rate of 50 mV/s (Fig. 6b).

Measurements were also performed at a rotating disk electrode (RDE) to calculate the number of electrons transferred in the catalytic electroreduction of dioxygen. The RDE response in air-saturated 1.0 M $HClO_4$ is illustrated in Fig. 7a. The number of electrons transferred during dioxygen reduction was calculated from the magnitude of the steady-state limiting currents which were taken at a fixed potential of -0.10 V on the plateau of the current-voltage curves. When the amount of O_2 reduction at the corrole modified electrode is controlled by mass transport alone, the relationship between the limiting current and rotation rate should obey the Levich equation given in Equation 1 [29], where n is the number of electrons transferred in the overall electrode reaction, F is the Faraday constant (96485 C.mol^{-1}), A is the electrode area (cm^2), D is the dioxygen diffusion coefficient (cm^2.s^{-1}), c is the bulk concentration of O_2 in 1.0 M $HClO_4$, v is the kinematic viscosity of the solution and ω is the angular rotation rate of the electrode (rad.s^{-1}).

$$J_{lev} = 0.62nFAD^{2/3}cv^{-1/6}\omega^{1/2} \quad (1)$$

When the reciprocal of the limiting current density is plotted against the reciprocal of the square root of the rotation rate, the resulting straight line (see Fig. 7b) obeys the Koutecky–Levich equation (Equation 2), where j is the measured limiting current density (mA.cm^{-2}), j_{lev} is the Levich current, and j_k is the kinetic current which can be obtained experimentally from the intercept of the Koutecky–Levich line in Fig. 7b.

$$1/j = 1/j_{lev} + 1/j_k \quad (2)$$

$$j_k = 10^3knF\Gamma c \quad (3)$$

The value of k (M^{-1}.s^{-1}) in Equations 2 and 3 is the second-order rate constant of the reaction which limits the plateau current, Γ is the surface concentration of corroles (mol.cm^{-2}) and the other terms have their usual significance as described previously. The slope of a plot obtained by linear regression can then be used to estimate the average number of electrons (n) involved in

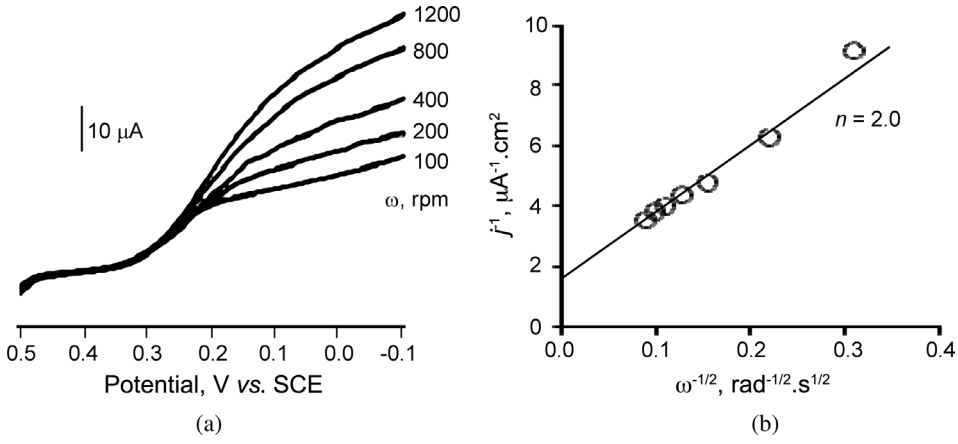

Fig. 7. (a) Current-voltage curve with electrode rotating rates (ω) indicated on each curve. Potential scan rate = 50 mV/s and (b) Koutecky-Levich plot for catalytic reduction of O_2 in 1.0 M $HClO_4$ saturated with air at a rotating EPPG disk electrode coated with $(Cl_2Ph)_3CorCo(PPh_3)$

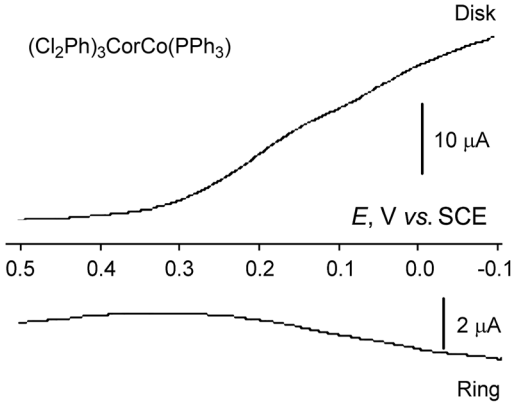

Fig. 8. Rotating ring-disk voltammograms of $(Cl_2Ph)_3CorCo(PPh_3)$ coated on EPPG electrode in 1.0 M $HClO_4$ saturated with air and the potential of the ring electrode maintained at 1.0 V. Rotation rate = 200 rpm and scan rate = 10 mV/s

the catalytic reduction of O_2. This analysis was carried out and the number of electrons transferred per dioxygen molecule (n) during the catalytic reduction of O_2 by the cobalt corrole was calculated.

A two electron transfer ($n = 2$) would generate 100% H_2O_2 while a four electron transfer ($n = 4$) would give 0% H_2O_2 and 100% H_2O. The Koutecky–Levich plot in Fig. 7b shows the number of electrons transferred (n) to be 2.0, which corresponds to 100% H_2O_2 produced. This indicates that the catalytic electroreduction of O_2 by $(Cl_2Ph)_3CorCo(PPh_3)$ is a $2e^-$ transfer process, giving H_2O_2 as the product rather than a $4e^-$ transfer process to produce H_2O.

The catalytic reduction of O_2 was also examined at an RRDE under the same solution conditions. The disk potential was scanned from 0.5 to -0.1 V at a rotation speed of 200 rpm while holding the ring potential constant at 1.0 V. This data is shown in Fig. 8 where the disk current begins to increase at about 0.30 V and a current maximum is reached at about 0.10 V. The anodic ring current increases throughout the range of the disk potentials where the disk current rises. Based on Equation 4 the amount of H_2O_2 formed upon the reduction of dioxygen was calculated as 98% under the given experimental conditions. The value are almost identical to that calculated using the Koutecky–Levich plot in Fig. 7b. The values of I_D and I_R in Equation 4 are the Faradic currents at the disk and ring electrodes, respectively. The intrinsic value of the collection efficiency (N) was determined to be 0.24 using the $[Fe(CN)_6]^{3-}/[Fe(CN)_6]^{4-}$ redox couple in 1.0 M KCl.

$$\%H_2O_2 = 100(2I_R/N)/(I_D+I_R/N) \quad (4)$$

In earlier studies, we examined the catalytic properties of several cobalt triarylcorroles containing the Cl, CH_3 or NO_2 substituents on the *para*-position of phenyl rings. For the catalytsts, the number of electron transferred (n) in the reduction of O_2 ranges form 2.2 to 3.0 depending upon the type of the substituent [11, 12]. However, in the current study, the value of n is exactly of 2.0 and the product of dioxygen reduction in 1.0 M $HClO_4$ is 100% H_2O_2. This is because that bulky *ortho*-Cl substituents on the *meso*-phenyl rings of the corrole result in steric hindrance which would block π–π interactions between macrocycles and prevent the formation of dimers which would facilite the 4-electron reduction to give an H_2O product [11, 22].

EXPERIMENTAL

Chemicals

Dichloromethane (CH_2Cl_2), benzonitrile (PhCN) and pyridine (Py) were purchased from Sigma–Aldrich Co. and used as received for electrochemistry and spectroelectrochemistry experiments. Tetra-*n*-butylammonium perchlorate (TBAP) was purchased from Sigma

Chemical or Fluka Chemika Co., recrystallized from ethyl alcohol, and dried under vacuum at 40 °C for at least one week prior to use.

5,10,15-tris(2,4-Dichlorophenyl)corrole cobalt triphenylphoshine, $(Cl_2Ph)_3CorCo(PPh_3)$ was synthesized according to the procedure described in literature [14, 30]. UV-vis (PhCN): λ_{max}, nm ($\varepsilon \times 10^{-4}$ $M^{-1}.cm^{-1}$) 383 (3.84), 411 (3.60), 557 (0.75), 580 (0.64). MS (MALDI-TOF): *m/z* 789.294, calcd. for $[M - PPh_3]^+$ 789.209.

Instrumentation

UV-visible spectra were recorded with a Hewlett–Packard Model 8453 diode array spectrophotometer. Cyclic voltammetry was carried out at 298 K using an EG&G Princeton Applied Research (PAR) 173 potentiostat/galvanostat or a Chi-730C Electrochemistry Work Station. A three-electrode system was used for cyclic voltammetric measurements and rotating disk voltammetry and consisted of a glassy carbon electrode or a graphite working electrode (Model MT134, Pine Instrument Co.), a platinum counter electrode and a homemade saturated calomel reference electrode (SCE). The SCE was separated from the bulk of the solution by a fritted glass bridge of low porosity which contained the solvent/supporting electrolyte mixture. High purity N_2 was used to deoxygenate the solution and kept over the solution during each electrochemical experiment.

The RRDE was purchased from Pine Instrument Co. and consisted of a platinum ring and a removable edge-plane pyrolytic graphite (EPPG) disk (A = 0.196 cm^2). A Pine Instrument MSR speed controller was used for the RDE and RRDE experiments. The Pt ring was first polished with 0.05 micron α-alumina powder and then rinsed successively with water and acetone before being activated by cycling the potential between 1.20 and -0.20 V in 1.0 M $HClO_4$ until reproducible voltammograms are obtained [31, 32].

The corrole catalyst was irreversibly adsorbed on the electrode surface by means of a dip-coating procedure described in the literature [9, 33]. The freshly polished electrode was dipped in a 1.0 mM catalyst solution of CH_2Cl_2 for 5 s, transferred rapidly to pure CH_2Cl_2 for 1–2 s, and then exposed to air where the adhering solvent rapidly evaporated leaving the corrole catalyst adsorbed on the electrode surface. All experiments were carried out under room temperature.

Thin-layer UV-visible spectroelectrochemical experiments were performed with a home-built thin-layer cell which has a light transparent platinum net working electrode. Potentials were applied and monitored with an EG&G PAR Model 173 potentiostat. Time-resolved UV-visible spectra were recorded with a Hewlett–Packard Model 8453 diode array spectrophotometer. High purity N_2 from Trigas was used to deoxygenate the solution and kept over the solution during each electrochemical and spectroelectrochemical experiment.

Theoretical calculations

Density-functional theory (DFT) calculations were performed with the Gaussian 09 program. Geometry optimizations were carried out in CH_2Cl_2 solution (dielectric constant, ε = 8.93) at the PCM-B3LYP/LanL2DZ functional and 6-31G(d) basis set [34–41]. The structures were confirmed to be minima by vibrational frequency analyses. All calculations were implemented in Gaussian 09, Revision D.01, Graphical outputs of the computational results were generated with the GaussView, ver. 5.09.

X-ray crystallography of $(Cl_2Ph)_3CorCo(PPh_3)$

Single-crystals of $(Cl_2Ph)_3CorCo(PPh_3)$ suitable for X-ray diffraction analysis were obtained in a mixture of dichloromethane and methanol, mounted on glass fiber and transferred to a Bruker Smart Apex CCD diffractometer. The unit cell parameters and crystal-orientation matrices were determined by least-squares refinements of all reflections. The intensity data were recorded as φ and ω scans with *k* offsets. The structure was solved by direct methods and followed by successive Fourier and difference Fourier syntheses. Refinements were carried out by full-matrix least-squares on *F* using SHELXL-2013 with anisotropic displacement parameters for all non-hydrogen atoms.

CONCLUSION

A cobalt corrole cotaining Cl substituents on *ortho*-positions of the three phenyl rings of the macrocycle was synthesized and the structure determined by X-ray crystal analysis. The compound is a selective catalyst for a 2-electron reduction of dioxygen and exclusively generates H_2O_2 as the product in acid media.

Acknowledgements

This work was supported by grants from the Natural Science Foundation of China (grants Nos. 21071067, 21301074) and the Robert A. Welch Foundation (KMK, grant No. E-680). We would like to thank Dr. Ruifa Zong for his kind help in X-ray crystal analysis.

Supporting information

Crystallographic data have been deposited at the Cambridge Crystallographic Data Centre (CCDC) under number CCDC-943276. Copies can be obtained on request, free of charge, *via* www.ccdc.cam.ac.uk/data_request/cif or from the Cambridge Crystallographic Data Centre, 12 Union Road, Cambridge CB2 1EZ, UK (fax: +44 1223-336-033 or email: data_request@ccdc.cam.ac.uk).

REFERENCES

1. Erben C, Will S and Kadish KM. In *The Porphyrin Handbook,* Vol. 2, Kadish KM, Smith KM and Guilard R. (Eds.) Academic Press: New York, 2000; pp 233–300.
2. Paolesse R. In *The Porphyrin Handbook*, Vol. 2, Kadish KM, Smith KM and Guilard R. (Eds.) Academic Press: San Diego, 2000; pp 201–232.
3. Aviv-Harel I and Gross Z. *Chem., Eur. J.* 2009; **15**: 8382–8394.
4. Thomas KE, Alemayehu AB, Conradie J, Beavers CM and Ghosh A. *Acc. Chem. Res.* 2012; **45**: 1203–1214.
5. McGown AJ, Badiei YM, Leeladee P, Prokop KA, DeBeer S and Goldberg DP. In *Handbook of Porphyrin Science*, Vol. 14, Kadish KM, Smith KM and Guilard R. (Eds.) Academic Press: New York, 2011; pp 525–594.
6. Lemon CM, Dogutan DK and Nocera DG. In *Handbook of Porphyrin Science*, Vol. 21, Kadish KM, Smith KM and Guilard R. (Eds.) Academic Press: New York, 2012; pp 1–143.
7. Aviv I and Gross Z. *Chem. Commun*. 2007; **20**: 1987–1999.
8. Lemon CM, Dogutan DK and Nocera DG. In *Handbook of Porphyrin Science*, Vol. 21, Kadish KM, Smith KM and Guilard R. (Eds.) Academic Press: New York, 2011; pp 1–143.
9. Kadish KM, Fremond L, Ou ZP, Shao JG, Shi CN, Anson FC, Burdet F, Gros CP, Barbe JM and Guilard R. *J. Am. Chem. Soc*. 2005; **127**: 5625–5631.
10. Kadish KM, Shao JG, Ou ZP, Fremond L, Zhan RQ, Burdet F, Barbe JM, Gros CP and Guilard R. *Inorg. Chem*. 2005; **44**: 6744–6754.
11. Ou ZP, Lü AX, Meng DY, Huang S, Fang YY, Lu GF and Kadish KM. *Inorg. Chem*. 2012; **51**: 8890–8896.
12. Li BH, Ou ZP, Meng DY, Tang JJ, Fang YY, Liu R and Kadish KM. *J. Inorg. Biochem*. 2014; **136**: 130–139.
13. Kadish KM, Shao JG, Ou ZP, Gros CP, Bolze F, Barbe JM and Guilard R. *Inorg. Chem*. 2003; **42**: 4062–4070.
14. Huang S, Fang YY, Lü AX, Lu GF, Ou ZP and Kadish KM. *J. Porphyrins Phthalocyanines* 2012; **16**: 958–967.
15. Kadish KM, Fremond L, Burdet F, Barbe JM, Gros CP and Guilard R. *J. Inorg. Biochem*. 2006; **100**: 858–868.
16. Guilard R, Jerome F, Gros CP, Barbe JM, Ou ZP, Shao JG and Kadish KM. *C. R. Acad. Sci. Series IIC: Chimie* 2001; **4**: 245–254.
17. Will S, Lex J, Vogel E, Adamian VA, Van Caemelbecke E and Kadish KM. *Inorg. Chem*. 1996; **35**: 5577–5583.
18. Adamian VA, D'Souza F, Licoccia S, Di Vona ML, Tassoni E, Paolesse R, Boschi T and Kadish KM. *Inorg. Chem*. 1995; **34**: 532–540.
19. Kadish KM, Adamian VA, Van Caemelbecke E, Gueletti E, Will S, Erben C and Vogel E. *J. Am. Chem. Soc*. 1998; **120**: 11986–11993.
20. Kadish KM, Koh W, Tagliatesta P, D'Souza F, Paolesse R, Licoccia S and Boschi T. *Inorg. Chem.* 1992; **31**: 2305–2313.
21. Kadish KM, Shao JG, Ou ZP, Gros CP, Bolze F, Barbe JM and Guilard R. *Inorg. Chem.* 2003; **42**: 4062–4070.
22. Kadish KM, Shen J, Fremond L, Chen P, El Ojaimi M, Chkounda M, Gros CP, Barbe JM, Ohkubo K, Fukuzumi S and Guilard R. *Inorg. Chem*. 2008; **47**: 6726–6737.
23. Collman JP, Kaplun M and Decreau RA. *Dalton Trans*. 2006; 554–559.
24. Schechter A, Stanevsky M, Mahammed A and Gross Z. *Inorg. Chem*. 2012; **51**: 22–24.
25. Kadish KM, Koh W, Tagliatesta P, D'Souza F, Paolesse R, Licoccia S and Boschi T. *Inorg. Chem*. 1992; **31**: 2305–2313.
26. Kadish KM, Lin XQ and Han BC. *Inorg. Chem*. 1987; **26**: 4161–4167.
27. Zhu WH, Sintic MS, Ou ZP, Sintic P, McDonal JA, Brotherhood PR, Crossley MJ and Kadish KM. *Inorg. Chem*. 2010; **49**: 1027–1038.
28. D'Souza F, Villard A, Van Caemelbecke E, Franzen M, Boschi T, Tagliatesta P and Kadish KM. *Inorg. Chem*. 1993; **32**: 4042–4048.
29. Bard AJ and Faulkner LR. *Electrochemical Methods: Fundamentals and Applications*, 2nd ed., John Wiley & Sons, Inc.: New York, 2001.
30. Ou ZP, Zhu JL, Lin WS, Fang YY and Lu GF. *Chem. J. Chinese U*. 2012; **33**: 1130–1137.
31. Conway BE, Angerstein-Kozlowska H, Sharp WBA and Criddle EE. *Anal. Chem.* 1973; **45**: 1331–1336.
32. Hsueh KL, Conzalez ER and Srinivasan S. *Electrochim. Acta* 1983; **28**: 691–697.
33. Shi C and Anson FC. *Inorg. Chem*. 1998; **37**: 1037–1043.
34. Lee C, Yang W and Parr RG. *Phys. Rev. B* 1988; **37**: 785–789.
35. Becke AD. *J. Chem. Phys.* 1993; **98**: 5648–5652.
36. Tomasi J and Persico M. *Chem. Rev*. 1994; **94**: 2027–2094.
37. Cossi M, Barone V, Cammi R and Tomasi J. *Chem. Phys. Lett*. 1996; **255**: 327–335.
38. Barone V, Cossi M and Tomasi J. *J. Chem. Phys*. 1997; **107**: 3210–3221.
39. Cossi M and Barone V. *J. Chem. Phys*. 1998; **109**: 6246–6254.
40. Barone V, Cossi M and Tomasi J. *J. Comput. Chem*. 1998; **19**: 404–417.
41. Cramer CJ and Truhlar DG. *Chem. Rev*. 1999; **99**: 2161–2200.